
Article:
Wang, Weiyu, Zhao, Xing orcid.org/0000-0003-4000-0446 and Niu, Shuangxia (2022) Predictive Pulse Injection Based Dual Inverter Complementary Sensorless Drive for 12/10 DC Vernier Reluctance Machine. IEEE Transactions on Power Electronics. pp. 8369-8378. ISSN 0885-8993

https://doi.org/10.1109/TPEL.2022.3150478

Predictive Pulse Injection based Dual-Inverter Complementary Sensorless Drive for 12/10 DC Vernier Reluctance Machine

Weiyu Wang, Xing Zhao, *Member, IEEE*, Shuangxia Niu, *Senior Member, IEEE*

***Abstract*- DC-Excited Vernier reluctance machine (DC-VRM) using 12-slot/10-pole-pair design, exhibits the advantages of small torque ripple and robust structure, which has good potential to be applied as an aerospace integrated starter/generator. By eliminating vulnerable position sensors, system reliability can be further improved by sensorless startup. However, driven by the traditional three-phase inverter, phase inductance of 12/10 DC-VRM becomes constant due to its complementary characteristic, which means the saliency effect in DC-VRM is obliterated, thereby sensorless operation using self-inductance detection cannot be applied. To release the machine saliency effect and further improve sensorless drive performance, a dual-inverter sensorless drive structure is introduced to reconstruct the machine saliency by using separated dual-three-phase inverters. The released series inductance model with mutual inductance coupling is established through a piecewise function, and an accurate position estimation method without finite element analysis or complex measurements is introduced. Moreover, by further analyzing the linearity of series inductance, the full-cycle inductance high-linearity range is composed of dual-inverter complementary features, thus position estimation accuracy can be guaranteed. Through this feature, a predictive position-based pulse injection sensorless drive method is proposed to improve acceleration performance with detection time reduction. Based on the predictive position, the detection pulses are only injected into one inverter whose corresponding phases are located at the inductance high-linearity range, thus decreasing the detection time and improving acceleration performance.**

I. INTRODUCTION

With the increasing concern of environmental protection and energy-saving, the research of more electrical aircraft (MEA) has attracted more attention [1-2]. Electrical machines, as the key component of integrated Starter/Generator (ISG) for MEA applications, are exposed to new challenges of higher power density, efficiency and reliability [3-5]. Although traditional permanent magnet (PM) synchronous machines have high power density and efficiency, the demagnetization risk of PM materials makes them unsuitable for high-temperature environments [6-7]. Therefore, developing reluctance machines without using vulnerable PMs [8-10] for aerospace ISG systems has been a hot research topic.

Switched reluctance machine (SRM) suffers from large torque ripple and noises [11], and controllable rectifier power converters are necessary for energy recycling. Doubly-fed doubly salient machine (DF-DSM) does not require controllable rectifiers in generator mode, and voltage regulation control can be easily achieved by adjusting field current. Unfortunately, its torque ripple is still unsatisfied due to the rich even-order flux harmonics and unbalanced magnetic distribution [12-13]. Compared to SRM and DF-DSM counterparts, more slot pole combinations can be used in DC-excited vernier reluctance machine (DC-VRM), especially the unit machine design with even-order rotor pole pair, which contributes to small torque ripple due to the elimination of even-order flux harmonics and the minimum cogging torque [14-15]. Thence, DC-VRM can be a better rare-earth-free solution to be applied as aerospace ISG.

By eliminating vulnerable position sensors, the reliability of the control system can be significantly improved by sensorless drive. For starter applications, sensorless start-up operations are mainly based on the machine saliency effect. The modulation method [16] and sense coil method [17] are easily influenced by signal noises, and the additional oscillator and demodulation circuits make them unsuitable for aerospace applications. Without additional hardware, the current waveform method [18-20] can detect the incremental inductance during the current chopping process by current waveform monitoring. However, with the increase of speed, the number of current chopping waves decreases, so the position detection accuracy is hard to be guaranteed. In addition, the saturation effect of the magnetic circuit needs to be considered in high load conditions [19]. In the pulse injection method, by injecting narrow detection pulses into idle phases, inductance can be detected indirectly, and the saturation effect can be ignored [20-21]. However, due to the half-cycle conduction principle of SRM, negative torque is generated, and non-idle phase inductance cannot be detected. So, to acquire the full-cycle inductance, different detection methods are combined [20].

Compared with the threshold conduction method [21] or sector estimation method [22,27-28], accurate position estimation can achieve adjustable conduction phase angle and optimal output torque. Through finite element analysis (FEA) or offline machine parameters measurements, position estimation fitting equation or 3-D table are stored in controller memory to achieve accurate position estimation [23-24]. However, these methods are easily affected by simulation errors,

This work was supported by the National Natural Science Foundation of China under Project 52077187 and in part by the Research Grant Council of the Hong Kong Government under Project PolyU 152143/18E and PolyU 152109/20E. (Corresponding author: Shuagnxia Niu)

Weiyu Wang and Shuangxia Niu are with the Department of Electrical Engineering, The Hong Kong Polytechnic University, Hong Kong, China. (e-mail: weiyu.wang@connect.polyu.hk; eesxniu@polyu.edu.hk)

Xing Zhao is with the School of Physics, Engineering and Technology, University of York, United Kingdom. (e-mail: xing.zhao@york.ac.uk;)

aging, or take up large memory sizes. So, position estimation methods with simplified measurements and without *prior* knowledge of the machine parameters attract more attention. To estimate the initial rotor position, the phase inductance is calculated by measuring the capacitor charging time in a bootstrap circuit, then the accurate initial position can be estimated in a parallelogram region [25]. The drawback is this method cannot be applied in a start-up operation. In [20], the authors extend the inductance vectors method to a low-speed range by detecting full-cycle inductances under light load conditions. In high load conditions, a second-order polynomial is required to reconstruct the unsaturated inductance by saturated inductance during the linear inductance region [19], thus complicating this method.

As DF-DSM is driven by a three-phase inverter, the detection pulses can be inserted into the acceleration pulses interval [26], thereby full-cycle inductance detection can be acquired by a single detection method, and the saturation effect can be ignored because of short duration detection pulses. However, based on the DF-DSM conduction principle, position detection and motor drive cannot be performed simultaneously, thus leads a communication delay. By reducing detection time, the reduced pulse injection method is an important optimization direction [22,27-28]. Furthermore, this problem can be also solved by accurate position estimation to ensure communication in time [29]. However, a position estimation blind zone named as boundary sector is caused by inductance nonlinearity, which makes the position estimation unreliable. To overcome this influence, a position prediction method in SRM [30] is introduced to DF-DSM [29] by replacing the inductance detection-based position estimation with instantaneous speed-based position prediction. However, the speed vibration and cumulative error cannot be overlooked, and the rotor initial position cannot be exactly acquired in the boundary sector.

The development of DC-VRM sensorless operation can create a solution that combines sensorless merits and low torque ripple performance. For DC-VRM using even rotor pole pair in unit machine design, the saliency effect of the machine is annihilated by traditional three-phase inverter drive, hence those advanced sensorless control methods by self-inductance detection cannot be applied. To solve this problem and further improve sensorless drive performance, three key issues are addressed. First, a parallel dual-inverter topology is introduced for DC-VRM to release the inherent saliency effect in self-inductance, thereby pulse injection sensorless drive can be applied. Second, an accurate position calculation method in series inductance dual-linearity range without *prior* knowledge is introduced. Moreover, the complementation feature of dual-inverter in position estimation is analyzed, and a predictive position-based pulse injection method (PPPIM) is proposed. The key is to apply the predictive position as a switch signal to redesign the detection pulses to be injected in the high-linearity series inductance ranges, thus decreasing the number of detection pulses to improve the acceleration performance. The arrangements of this paper are as follows. In Section II, the mathematical model of DC-VRM and the dual-inverter drive structure are introduced. In Section III, the series inductance model is established. In Section IV, the high-precision position estimation method is introduced. In Section V, PPPIM is proposed. In Section VI, experimental results are presented. Finally, some conclusions are drawn.

II. Configuration of 12/10 DC-VRM

A. Dual-inverter Sensorless Drive System

As shown in Fig .1, integrated Starter/Generator (ISG) integrates electric starting function and power generation function into one machine, thereby a smaller size, lighter weight and lower cost solution can be achieved. Fig .2 shows the structure of 12/10 DC-VRM that DC field coils and AC armature coils are integrated into the stator slots, respectively. All the DC field coils are connected in series to form one single DC field winding. As shown in Fig .3, in a traditional three-phase inverter drive system, two sets of armature coils that have 180° phase differences are reversely cascaded to form a single-phase winding. Fig .4 shows the FEA result that phases A and D are reversely connected to form the phase winding of U. All the odd-order harmonic self-inductances are canceled when they are superimposed. Therefore, the saliency of the machine is annihilated, regardless of its salient-pole structure and associated variable self-inductance, thereby reliable self-inductance detection-based sensorless drive cannot be applied.

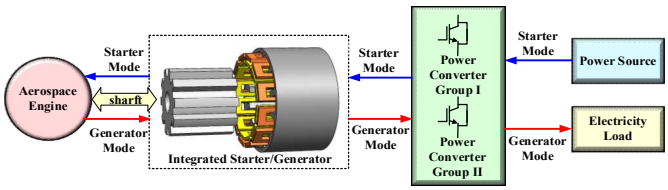

Fig .1. Aerospace integrated starter and generator system.

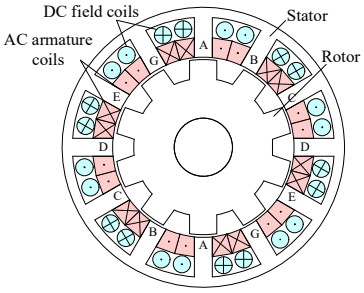

Fig. 2. Structure of 12/10 DC-VRM.

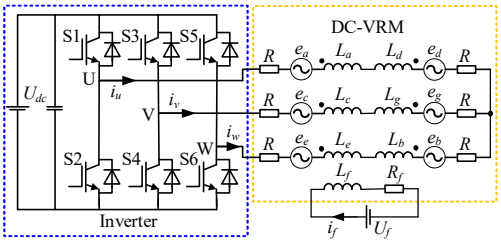

Fig. 3. Traditional three-phase inverter drive for DC-VRM.

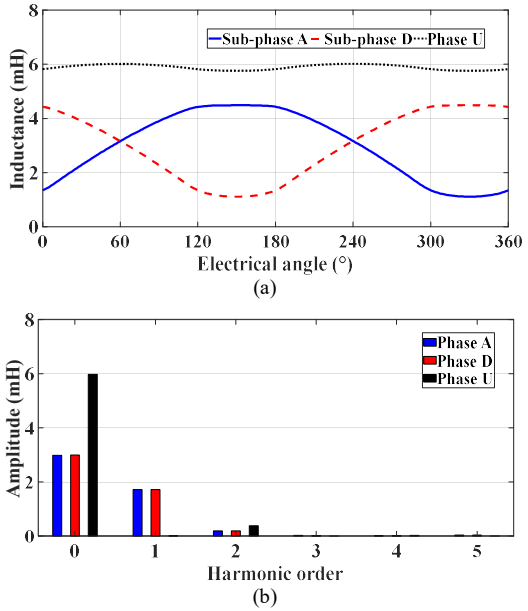

Fig. 4. (a) Phase inductances of A, D and U. (b) Harmonics distributions.

To avoid the annihilation in phase self-inductance, a parallel dual-inverter drive system is adopted to separate the coils into two groups, thus recovering the inherent saliency. The parallel dual-inverter drive system is described in Fig .5.

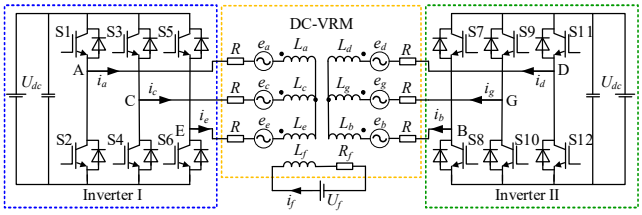

Fig. 5. Dual-inverter drive for DC-VRM.

B. Mathematical Model

The current and inductance equations can be expressed as

$$I=[i_a \quad i_b \quad i_c \quad i_d \quad i_e \quad i_g \quad i_f]^T \tag{1}$$

$$L=\begin{bmatrix} L_a & L_{ab} & L_{ac} & L_{ad} & L_{ae} & L_{ag} & L_{af} \\ L_{ab} & L_b & L_{bc} & L_{bd} & L_{be} & L_{bg} & L_{bf} \\ L_{ac} & L_{bc} & L_c & L_{cd} & L_{ce} & L_{cg} & L_{cf} \\ L_{ad} & L_{bd} & L_{cd} & L_d & L_{de} & L_{dg} & L_{df} \\ L_{ae} & L_{be} & L_{ce} & L_{de} & L_e & L_{eg} & L_{ef} \\ L_{ag} & L_{bg} & L_{cg} & L_{dg} & L_{eg} & L_g & L_{gf} \\ L_{af} & L_{bf} & L_{cf} & L_{df} & L_{ef} & L_{gf} & L_f \end{bmatrix} \tag{2}$$

where I is the current matrix, i_a, i_b, i_c, i_d, i_e and i_g are the phase currents, i_f is the field current, L is the inductance matrix, L_{af}, L_{bf}, L_{cf}, L_{df}, L_{ef} and L_{gf} are the mutual inductances between phase windings and the field winding, L_a, L_b, L_c, L_d, L_e and L_g are the self-inductances, L_{ab}, L_{ac}, L_{ad}, L_{ae}, L_{ag}, L_{bc}, L_{bd}, L_{be}, L_{bg}, L_{cd}, L_{ce}, L_{cg}, L_{de}, L_{dg} and L_{eg} are the mutual inductances between phases, L_f is the self-inductance of the field winding. Taking phase A as an example, the torque components under current excitation can be expanded as

$$T_a=i_a i_f \frac{dL_{af}}{d\theta}+\frac{1}{2}i_a^2\frac{dL_a}{d\theta}+\frac{1}{2}i_f^2\frac{dL_f}{d\theta} \tag{3}$$

where θ is the electrical angle. The first term is the major component of the excitation torque produced by the mutual inductance between DC field winding and the armature winding. The second term is the reluctance torque produced by variation of phase self-inductance. Due to bipolar current excitation, the average reluctance torque in the whole electrical period is zero. The third term is the cogging torque produced by DC field winding. As L_f keeps constant in the whole electrical period, the cogging torque can be neglected.

III. Pulse Injection-based Series Inductance Detection

A. Pulse Injection-based Series Inductance Detection

For reluctance machines with doubly salient structures, the air gap permeance changes with rotor position periodically, leading to the variation of phase inductance simultaneously. This gives the advantage of a sensorless operation by detecting winding inductances. Therefore, by injecting detection pulses into phase windings, self-inductance can be indirectly detected to estimate the rotor position. As shown in Fig .6, a short-duration detection pulse is injected by switching on transistors S1 and S4. During this process, the instantaneous conduction loop is the series connection of phases A and C with mutual inductance coupling between them, and the voltage equation can be expressed as

$$U_{dc}=(L_a+L_c-2L_{ac})\frac{di_a}{dt}+i_a\frac{d(L_a+L_c-2L_{ac})}{d\theta}\omega+i_aR \tag{4}$$

where ω is the rotor angular velocity. During zero or low speed-range, ω is zero or quite small, back-electromotive force (back-EMF) can be ignored [26,28]. In addition, the short-duration detection pulse leads to a small response current, then the winding voltage drop can also be ignored [20,26,28]. Voltage equation can be further simplified as

$$U_{dc}=(L_a+L_c-2L_{ac})\frac{di_a}{dt} \tag{5}$$

The series inductance can be described as

$$L_{p+q}=L_p+L_q-2L_{pq}=\frac{U_{dc}\Delta t}{I_{p+q}} \quad (p,q=A,B,C,D,E,G, \quad p\neq q) \tag{6}$$

where Δt is the detection pulse width.

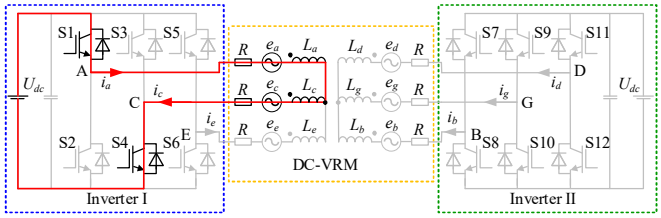

Fig. 6. Dual-inverter pulse injection equivalent circuit.

B. Series Inductance Characteristics

Through the above analysis, the value detected by the detection pulse is a series inductance with mutual inductance coupling. To further analyze the mutual inductance coupling

between armature windings, the FEA results when phase A is excited at different rotor positions are compared in Fig .7. The mutual inductance between the armature windings is related to the cross-sectional area of the magnetic circuit formed by the series-connected dual-phases, which is affected by the meshing degree of the series dual-phases simultaneously.

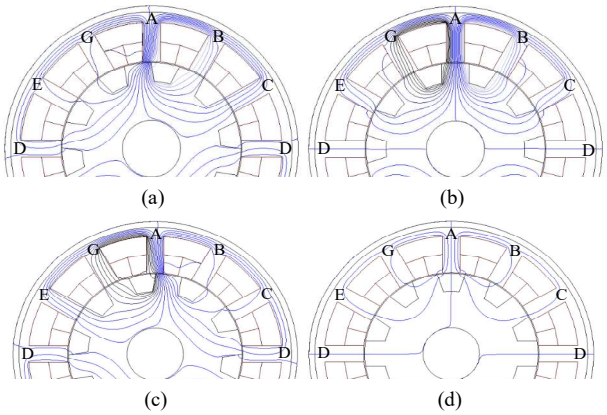

Fig. 7. Flux distributions when phase A is excited at different positions. (a) 60°. (b) 150°. (c) 240°. (d) 330°.

The series inductance is established in Fig .8, which can be represented by a piecewise function (7). Due to the influence of mutual inductance, the rising or falling stages are divided into two parts with different slopes.

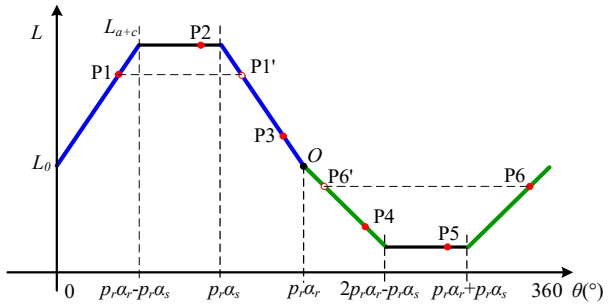

Fig. 8. DC-VRM series inductance model.

$$L(\theta)=\begin{cases} k_1\theta + L_0, & \theta\epsilon[0, p_r\alpha_r - p_r\alpha_s] \\ k_1 p_r(\alpha_r-\alpha_s)+L_0, & \theta\epsilon[p_r\alpha_r - p_r\alpha_s, p_r\alpha_s] \\ -k_1\theta + +3k_1 p_r(\alpha_r-\alpha_s)+L_0, & \theta\epsilon[p_r\alpha_s, p_r\alpha_r] \\ -k_2\theta+3k_2 p_r(\alpha_r-\alpha_s)+L_0 & \theta\epsilon[p_r\alpha_r, 2p_r\alpha_r - p_r\alpha_s] \\ -k_2 p_r(\alpha_r-\alpha_s)+L_0, & \theta\epsilon[2p_r\alpha_r - p_r\alpha_s, p_r\alpha_r + p_r\alpha_s] \\ k_2\theta - 6k_2 p_r(\alpha_r-\alpha_s)+L_0, & \theta\epsilon[p_r\alpha_r + p_r\alpha_s, 360] \end{cases} \quad (7)$$

where p_r is the rotor pole number, α_r and α_s are rotor pole arc and stator pole arc, which are designed as 18° and 12°, respectively. k_1 and k_2 are the slopes of dual-linearity ranges, respectively. Due to the symmetrical distribution of the magnetic circuit of each phase in the DC-VRM, the series inductances formed by different phases have the same amplitudes but are accompanied by 60° phase shifts between adjacent phases. The position of the rotor sector can be determined by comparing the magnitudes of the series inductances, which can be found in Table I.

TABLE I
RELATION BETWEEN ELECTRICAL ANGLE, SERIES-INDUCTANCES, CONDUCTION PHASES AND ROTOR SECTOR

θ (°)	Inductance relation	Conduction phases	Sector
0-60	$Max(L_{p+q})= L_{b+d}$	A, D, B, E	I
60-120	$Max(L_{p+q})= L_{a+c}$	A, D, C, G	II
120-180	$Max(L_{p+q})= L_{b+g}$	B, E, C, G	III
180-240	$Max(L_{p+q})= L_{a+e}$	A, D, B, E	IV
240-300	$Max(L_{p+q})= L_{d+g}$	A, D, C, G	V
300-360	$Max(L_{p+q})= L_{c+e}$	B, E, C, G	VI

The characteristics of the series inductance are summarized as follows. According to the phase interval of the six series inductances formed by the dual three-phase, the detection of the dual three-phase series inductances by pulse injection can be regarded as six-time discrete samplings of the series inductance function $L(\theta)$. As shown in Fig .8, P1, P2, P3, P4, P5 and P6 represent the sampling points with 60° intervals between adjacent sampling points. Among them, P1, P3, P4, P6 are in the rising or falling stage of series inductance, which contains a clear correspondence between inductance amplitude and position. While at the sampling points of P2 and P5, the series inductance fluctuation is not obvious. Therefore, this information is only suitable for sector estimation, but not for accurate position estimation. Meanwhile, according to the characteristics of symmetry of series inductance, P1 and P6 can be mirrored to the points P1' and P6', respectively, thereby enough sampling points can be obtained in the dual-linear intervals for accurate position estimation.

IV. Series Inductance Dual-Linearity-Range-Based Position Estimation

According to the characteristics of the series inductance analyzed in the previous chapter, the linear intervals l_1 and l_2 of the series inductance are redefined in an orthogonal coordinate system, which can be found in Fig .9. Therefore, the detection points at P2 and P5 with less position-related information are not introduced for accurate position estimation. Only the detection points located at the $L(\theta)$ linearity ranges are applied.

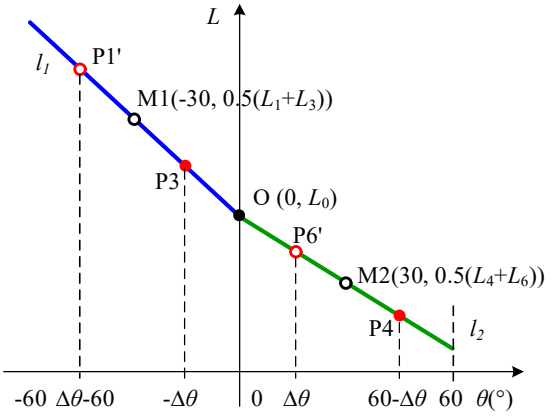

Fig. 9. Series inductance dual-linearity range.

The electrical angle can be expressed as

$$\theta=60(s\text{-}1)+\Delta\theta, \qquad s=1,2,3,4,5,6 \tag{8}$$

where s is the sector, $\Delta\theta$ is the bias electrical angle. Then, the coordinates of the sampling points can be decided as P1' ($\Delta\theta$-60, L_1), P3(-$\Delta\theta$, L_3), P6' ($\Delta\theta$, L_6) and P4(60-$\Delta\theta$, L_4). The expression of the piecewise linear interval of series inductance is shown in the formula (9).

$$\begin{cases} l_1=-k_1\theta+L_0=\dfrac{L_3-L_1}{60-2\Delta\theta}\theta_1+L_0, & \theta_1\in[-60,0] \\ l_2=-k_2\theta+L_0=\dfrac{L_4-L_6}{60-2\Delta\theta}\theta_2+L_0, & \theta_2\in[0,60] \end{cases} \tag{9}$$

where L_1, L_3, L_4 and L_6 are the detected inductances at the points P1, P3, P4 and P6, respectively. Furthermore, the coordinates of the midpoints of the two-line segments can be easily obtained as M1 (-30, 0.5(L_1+L_3)) and M2 (30, 0.5(L_4+L_3)). By substituting M1 and M2 into formula (9), $\Delta\theta$ can be solved as

$$\Delta\theta=30-\frac{(L_4-L_6)\theta_2-(L_3-L_1)\theta_1}{2(l_2-l_1)}=\frac{60(L_6-L_3)}{L_6+L_4-L_3-L_1} \tag{10}$$

To further improve the accuracy of position estimation, re-sampling can be applied to reduce the estimation error.

$$\Delta\theta=\frac{1}{n}\sum_1^n\frac{60(L_{6n}-L_{3n})}{L_{6n}+L_{4n}-L_{3n}-L_{1n}} \tag{11}$$

where n is the re-sampling times. In this series inductance modeling method, the inductance model can be accurately obtained in the process of initial position detection without FEA. As shown in (12), the parameters of k_1, k_2 and L_0 can be deduced at a certain initial position to simplify the position estimation process during the acceleration stage. Therefore, the series inductance dual-linearity ranges can be independently solved.

$$\begin{cases} k_1=-\dfrac{L_3-L_1}{60-2\Delta\theta} \\ k_2=-\dfrac{L_4-L_6}{60-2\Delta\theta} \\ L_0=\dfrac{-30(L_3-L_1)}{60-2\Delta\theta}-\dfrac{L_3+L_1}{2} \end{cases} \tag{12}$$

So, it is unnecessary to detect full-phase inductances for position estimation. The position calculation in the high-linearity interval of the inductance will obtain more reliable position estimation accuracy. Through FEA and linear fitting, the linearities of the l_1 and l_2 are compared in Table II. SSE, RMSE, R-square and Adjusted R-square are the acronyms of the sum of squares due to error, root mean squared error, coefficient of determination and degree-of-freedom adjusted coefficient of determination, respectively. The linearity of the inductance in the l_1 interval is higher, which means the linear function modeling is more accurate, and the reliability of the position estimation based on l_1 is higher.

TABLE II
COMPARISON OF LINEARITY CHARACTERISTICS

	SSE	RMSE	R-square	Adj-sq
l_1	0.0126	0.0290	0.9987	0.9986
l_2	0.0952	0.0797	0.9761	0.9745

V. Predicted Position-based Pulse Injection Sensorless Drive with Dual-Inverter Complementary Strategy

A. Full-phase Sequential Pulse Injection Method

The full-phase sequential pulse injection method (Full-phase SPIM) can be seen as a typical pulse injection sensorless drive method that injects detection pulses in each phase in sequence to acquire position information. The schematic diagram of the acceleration process of full-phase SPIM is shown in Fig .10. Only one series phase conducts at the same time, thus the peak current sampling is not affected by mutual inductance between different pairs of series inductances. An operation cycle is defined as the period from t_1 to t_5 that consists of alternative detection pulses and acceleration pulses. First, the detection pulse sequence is injected from t_1 to t_2, and the resultant currents are registered. After full phases are detected, the rotor position can be estimated between t_2 and t_3. Then the conduction phases are determined, and further acceleration pulses are injected during the period from t_3 to t_4. By completing the demagnetization process between t_4 and t_5, a new round of detection pulses is injected from t_5.

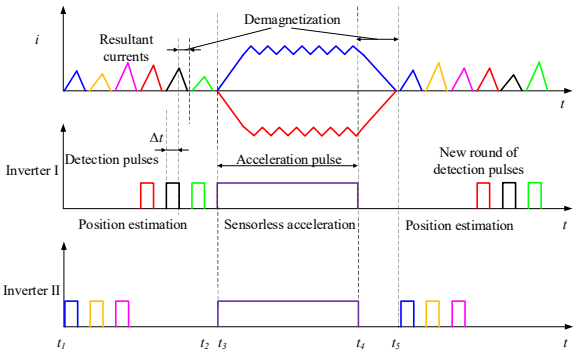

Fig. 10. Schematic diagram of full-phase sequential pulse injection.

B. Dual-Inverter Complementary Feature on Position Estimation

For the start-up process, the detection duration is desired to be decreased to reduce the commutation delay and increase the duty cycle of the acceleration pulse, thus improving the acceleration performance. To reduce detection time and obtain accurate position estimation simultaneously, a dual-inverter complementary feature on position estimation is analyzed. The three phases of Inverter I can be regarded as having a 180° phase shift with those of Inverter II. According to the analysis of the linearity of the linear interval of the series inductance, the high linearity interval l_1 and the low linearity interval l_2 of the series inductance are alternately distributed in a single three-phase, which can be found in Fig .11. The distribution law of the high linearity interval and the low linearity interval of the series inductance is opposite. Therefore, the full-cycle accurate position estimation can be obtained by integrating the position detection information of the dual inverters.

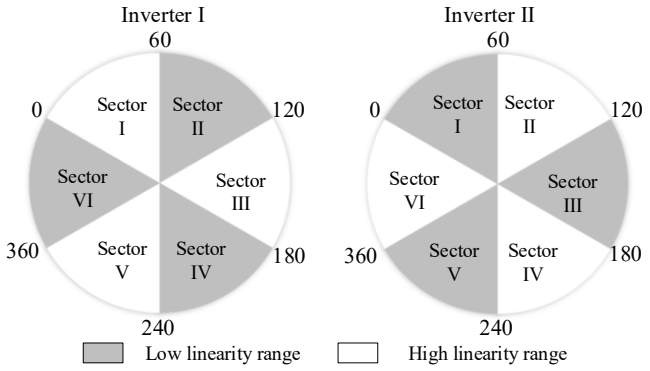

Fig. 11. Dual-inverter complementary feature of position estimation.

C. Predictive Position-based Pulse Injection Method

Based on the dual-inverter complementary feature, a predictive position-based pulse injection method (PPPIM) is proposed. The position prediction method in [30] is introduced to select inverters to inject detection pulses at the next detection period, thus guaranteeing the detection pulses are injected during the high-linearity inductance range. In this way, the inverter at the low-linearity range does not inject detection pulses, thus decreasing the detection time. Since the pulse injection method is discrete position detection, the speed can be estimated by twice detection positions and their detection time interval ΔT_d.

$$\omega_e = \frac{\theta(k)-\theta(k\text{-}1)}{\Delta T_d} \tag{13}$$

where ω_e is the estimated speed, $\theta(k)$ is the k_{th} sampled position, $\theta(k\text{-}1)$ is the $(k\text{-}1)_{\text{th}}$ sampled position. The $(k+1)_{\text{th}}$ position can be estimated as

$$\theta(k+1)=\theta(k)+\omega_e \Delta T_d \tag{14}$$

Then the pulse injection selection command for Inverter I $f(\theta(k+1))$ can be decided by $\theta(k+1)$,

$$f(\theta(k+1)) = \begin{cases} 1 & , \ \theta_e \in [0,60) \cup [120,180) \cup [240,300) \\ 0 & , \theta_e \in [60,120) \cup [180,240) \cup [300,360) \end{cases} \tag{15}$$

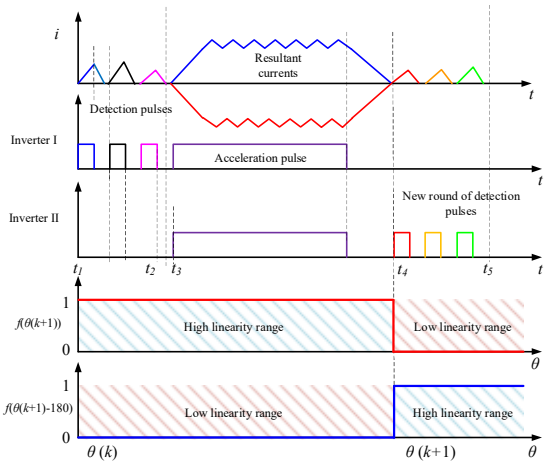

Fig. 12. Schematic diagram of predicted position-based pulse injection method.

The detection pulses are injected by Inverter I once $f(\theta(k+1))$ equals 1. Apparently, for Inverter II, the pulse injection command is $f(\theta(k+1)\text{-}180)$. The schematic diagram of the PPPIM with dual-inverter complementation feature is shown in Fig .12. The detection pulses are redesigned based on the predictive position to guarantee the detection pulses are injected during the inductance high-linearity range.

D. Position Estimation Error Analysis

The predictive position method can obtain continuous position estimation, which can also be used to calculate the position in the boundary sector caused by inductance nonlinearity [29]. But in essence, this method is a position estimation based on the instantaneous estimated speed, which is easily affected by speed fluctuations. Also, this method may be affected by the cumulative error. As shown in Fig .13, although this method can describe the position information during the boundary sector, if the position detection cannot be updated accurately in time, the position estimation cumulative error may seriously increase, which means accurate position should be updated in time.

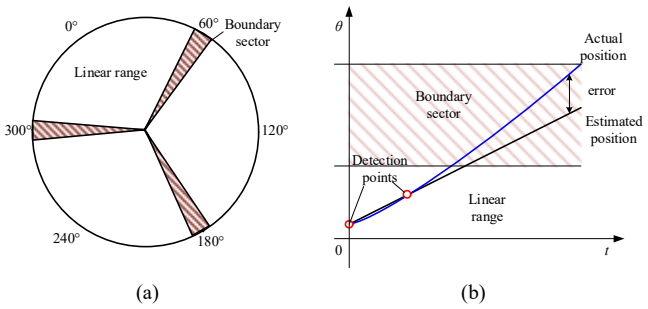

Fig. 13. (a) Boundary sector. (b) Estimation error.

In the proposed method, the predictive position is not introduced to replace the estimated position. Instead, it is only applied as a switching signal to select detection pulses to ensure they are reasonably injected into the high-linearity interval in dual-inverters. As shown in Fig .14, position information can be updated in time, thus avoiding cumulative error effectively, which significantly improves sensorless drive reliability.

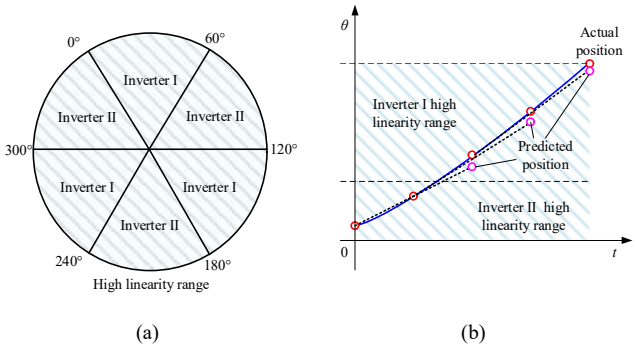

Fig. 14. (a) Dual-inverter complementation high-linearity range. (b) Estimation error.

E. Sensorless Startup Strategy as ISG

Fig .15 shows the flowchart of the sensorless startup as an ISG. First, detection pulses are injected from the dual-inverter to detect the series inductance, then the initial position can be estimated at $\theta(k\text{-}1)$ by the dual-linearity range calculation method. The conduction phases are decided, and the acceleration pulses are injected to drive the machine. A new round of dual-inverter detection pulses is inserted to detect $\theta(k)$ position, and then the speed can be estimated to predict $\theta(k+1)$ position. In the next detection cycle, the injection pulse can be selected through $f(\theta(k+1))$, thereby the position estimation can be conducted during the predictive high-linearity range. Once the speed is large enough, the system can be switched to generator mode.

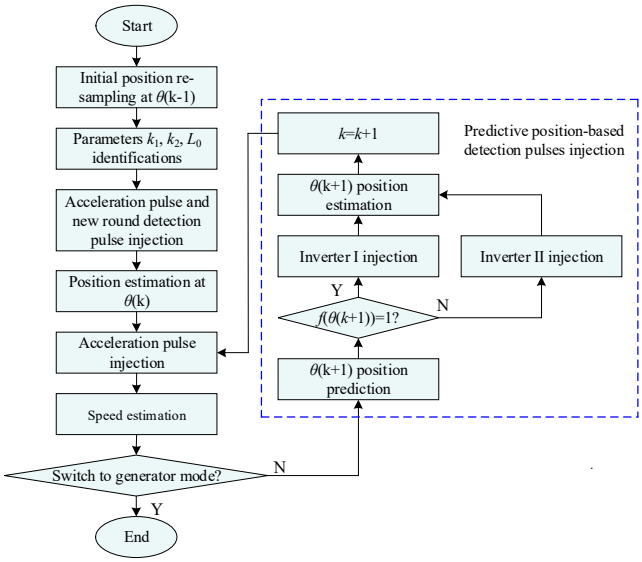

Fig. 15. Flowchart of the proposed sensorless startup strategy.

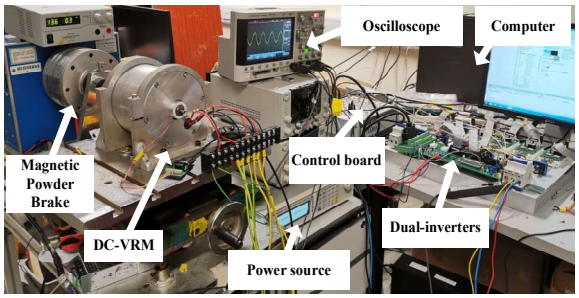

Fig. 16. Experimental setup of the proposed DC-VRM drive system.

VI. Experimental Results

A. Experimental Setup

As the experimental setup is shown in Fig .16, the sensorless control is performed based on a real-time control platform of a dSPACE MicroLabBox with a sampling rate of 50kHz. Parameters can be monitored by a PC or an oscilloscope. Dual-inverters are applied to drive the DC-VRM. The field winding is excited by the DC power source to establish the excitation magnetic field. A coaxial magnetic powder brake is connected to the DC-VRM.

B. Initial Position Detection

As shown in Fig .17, to obtain the initial position, detection pulses are sequentially injected to indirectly detect the series inductances. Through the dual-linearity position estimation method, the initial position can be accurately obtained.

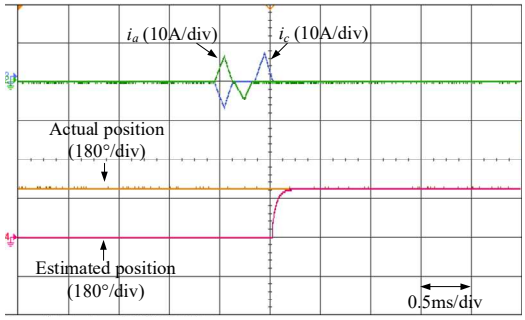

Fig. 17. Pulse injection initial position estimation.

To further verify the accuracy of the series inductance model, the rotor is manually placed at different initial positions and current samplings are performed to reconstruct each series inductance in the whole electrical angle period. With the series inductance dual-linearity position estimation method, the estimated position is compared with the actual position in Fig .18(a). As shown in Fig .18(b), the position estimation error can be controlled with the range of 5° electrical angle, corresponding to 0.5° of rotor angle in the whole electrical period.

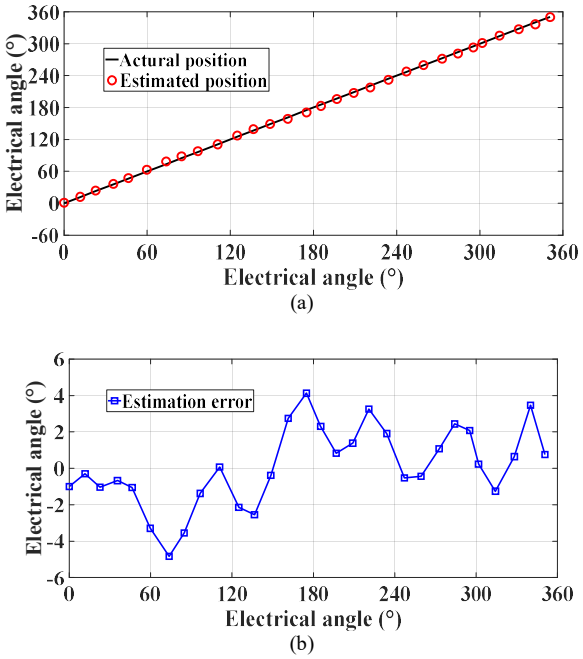

Fig. 18. (a) Position estimation in an electrical angle period. (b) Estimation error.

The measured inductance and the established inductance model are compared in Fig 19. The parameters of k_1, k_2 and L_0 are calculated as 0.044, 0.012 and 5.8, respectively. Accurate fitting results can be found in the high-linearity inductance range, which means, in this series inductance modeling method, the inductance high-linearity range can be accurately reproduced. The fitting result of the low linearity interval of the inductance is relatively lower than the high linearity interval, but a certain accuracy can still be guaranteed. The worst situations can be found in inductance flat top and flat bottom areas. That is because horizontal straight lines are introduced to simplify the inductance modeling process in flat ranges. Although the fitting results in these ranges are poor, the position estimation results are not influenced. That is because the proposed PPPIM only calculates rotor position in the high-linearity inductance range.

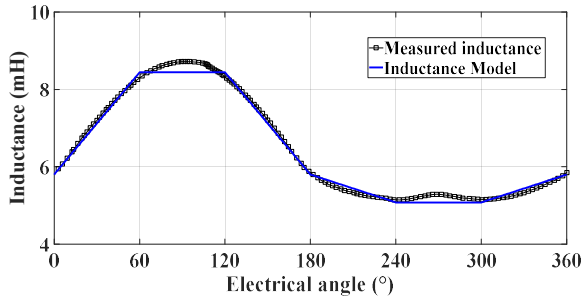

Fig. 19. Measured inductance and established inductance model of DC-VRM.

The position estimation errors from the high-linearity inductance range and low-linearity inductance range are compared in Fig .20. It is clear to see that the position estimation at the high-linearity inductance range can acquire a higher position estimation accuracy compared with the low-linearity range. The position estimation error can be controlled within the range of 2.5°, compared with 6.5° in that of the low-inductance range.

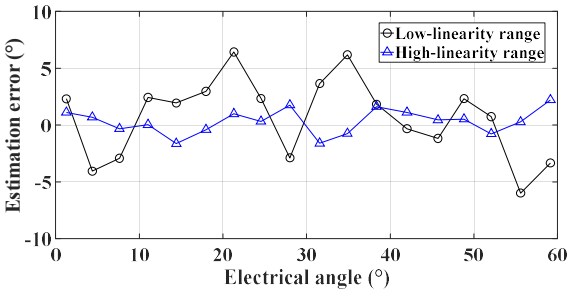

Fig. 20. Position estimation errors of high-linearity inductance range and low-linearity inductance range.

C. Predictive Position-based Reduced Pulse Injection Sensorless Drive with a Dual-inverter Complementary Feature

The full-phase SPIM is compared with the proposed PPPIM in Fig .21. Based on the pulse injection width selection rules and experiments [20,29], the detection pulse width and acceleration pulse width are designed as 0.1ms and 1ms, respectively. The load torque is 1Nm. Based on the predictive position, the detection pulses are only injected by a single inverter whose related phases are located at the high linearity inductance range, thereby reducing the detection time and obtaining higher acceleration performance. By the proposed method, the rotor speed can reach 380rpm in 1 second compared with 200rpm in the full-phase SPIM. The proposed PPPIM based dual-inverter complementary sensorless drive method can reduce detection pulses injection by predictive position to improve acceleration speed. Also, reliable position estimation accuracy can be acquired in the high-linearity inductance range by dual-inverter complementary feature. Therefore, the acceleration performance in the startup process can be significantly improved by the proposed method.

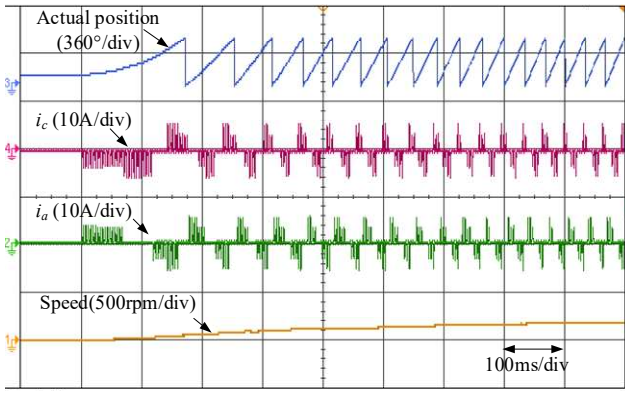

(a)

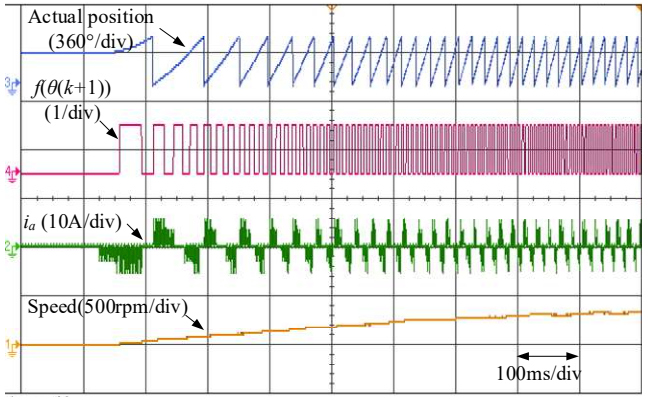

(b)

Fig. 21. Acceleration performance (a) Full-phase SPIM. (b) PPPIM.

The position estimation error by the proposed PPPIM is shown in Fig .22. In the whole acceleration process, the position estimation error can be controlled within the range of 15°. By increasing the load torque to 1.5Nm, the acceleration performance is shown in Fig .22 (b). It is clear to see that the position estimation does not show a remarkable difference, but with a reduction in acceleration speed. That's because this acceleration method works with the constant torque zone. The estimated position is introduced into phase communication to guarantee the reliability of the sensorless drive. The specific parameters of the prototype machine can be found in Table III.

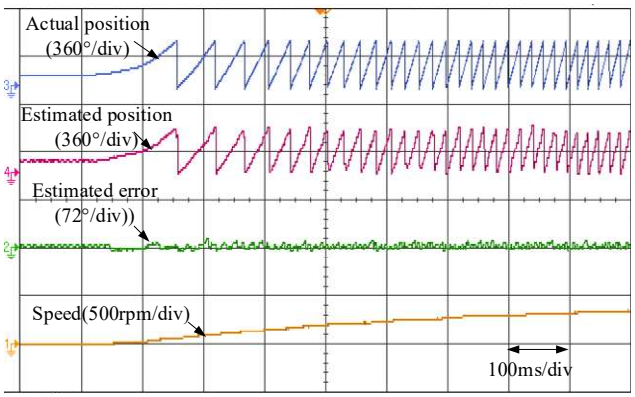

(a)

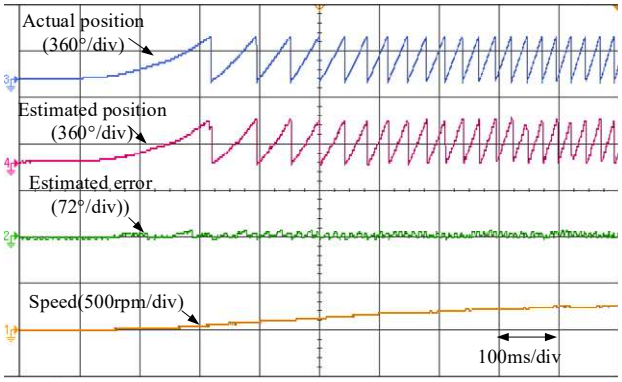

(b)

Fig. 22. Sensorless acceleration under load condition. (a) 1Nm. (b) 1.5Nm.

TABLE III
SPECIFIC PARAMETERS FOR THE DC-VRM

Symbol	Parameter	Unit	Value
α_s	Stator pole arc	°	12
α_r	Rotor pole arc	°	18
N_{dc}	Turns of each DC coil	-	48
N_{ac}	Turns of each AC coil	-	48
R	Sub-phase winding resistance	Ω	0.7
R_f	Field winding resistance	Ω	4.2
	Rated torque	Nm	2.4
	Rated speed	r/min	450
	Rated power	W	600

CONCLUSION

This paper proposes a predictive position-based reduced pulse injection sensorless drive method for 12/10 DC-VRM with the dual-inverter complementary feature. To improve system reliability by the sensorless startup, a dual-inverter drive system is introduced to reconstruct the machine saliency effect by separating the constant phase inductance into two variable inductance components, thus achieving pulse injection inductance detection sensorless drive. Then, the series inductance model is established, and the dual-linearity range accurate position estimation strategy is illustrated. High-precision position estimation can be acquired without *prior* knowledge. Furthermore, to improve acceleration performance, a reduced-pulse injection sensorless drive method with the guidance of predictive position is proposed. Based on the predictive position, the detection pulses are injected during series inductance high-linearity range, thus keeping detection accuracy, and reducing detection time simultaneously. The acceleration performance can be significantly improved that the rotor speed can reach 380rpm in 1 second. A solution that combines sensorless drive merits and low torque ripple is achieved. which has good potential to be applied as an aerospace ISG.

ACKNOWLEDGMENT

This work was supported by the National Natural Science Foundation of China under Project 52077187 and in part by the Research Grant Council of the Hong Kong Government under Project PolyU 152143/18E and PolyU 152109/20E.

REFERENCES

[1] B. Sarlioglu and C. T. Morris, "More Electric Aircraft: Review, Challenges, and Opportunities for Commercial Transport Aircraft," *IEEE Trans. Transp. Electrif.*, vol. 1, no. 1, pp. 54-64, June 2015.

[2] V. Madonna, P. Giangrande and M. Galea, "Electrical Power Generation in Aircraft: Review, Challenges, and Opportunities," *IEEE Trans. Transp. Electrif.*, vol. 4, no. 3, pp. 646-659, Sept. 2018.

[3] A. Griffo, R. Wrobel, P. H. Mellor and J. M. Yon, "Design and Characterization of a Three-Phase Brushless Exciter for Aircraft Starter/Generator," *IEEE Trans Ind. Appl.,* vol. 49, no. 5, pp. 2106-2115, Sept.-Oct. 2013.

[4] R. Bojoi, A. Cavagnino, A. Tenconi and S. Vaschetto, "Control of Shaft-Line-Embedded Multiphase Starter/Generator for Aero-Engine," *IEEE Trans. Ind. Electron*., vol. 63, no. 1, pp. 641-652, Jan. 2016.

[5] N. Jiao, C. Sun, X. Zhang, X. Duan and W. Liu, "Double-Side Voltage-Behind-Reactance Model of Brushless Exciter in Aircraft Wound-Rotor Synchronous Starter-Generator Considering Magnetic Saturation," *IEEE Trans. Energy Convers.*, vol. 36, no. 3, pp. 2358-2369, Sept. 2021.

[6] P. B. Reddy, A. M. El-Refaie, K. K. Huh, J. K. Tangudu and T. M. Jahns, "Comparison of interior and surface PM machines equipped with fractional-slot concentrated windings for hybrid traction applications," *IEEE Trans. Energy Convers*., vol. 27, no. 3, pp. 593-602, Sept. 2012.

[7] M. Cheng, W. Hua, J. Zhang and W. Zhao, "Overview of Stator-Permanent Magnet Brushless Machines," *IEEE Trans. Ind. Electron*., vol. 58, no. 11, pp. 5087-5101, Nov. 2011.

[8] I. Boldea, L. N. Tutelea, and D. Dorrell, "Automotive electric propulsion systems with reduced or no permanent magnets: an overview," *IEEE Trans. Ind. Electron*., vol. 61, no. 10, pp. 5696-5711, Oct. 2014.

[9] X. Zhao and S. Niu, "Design of a Novel Parallel-Hybrid-Excited Vernier Reluctance Machine with Improved Utilization of Redundant Winding

Harmonics," *IEEE Trans. Ind. Electron.*, vol. 65, no. 11, pp. 9056-9067, Nov. 2018.
[10] D. Xiao, J. Ye, G. Fang, Z. Xia, X. Wang and A. Emadi, "Improved feature-position-based sensorless control scheme for SRM drives based on nonlinear state observer at medium and high speeds," *IEEE Trans. Power Electron.*, vol. 36, no. 5, pp. 5711-5723, May 2021.
[11] Y. Jin, B. Bilgin, and A. Emadi, "An extended-speed low-ripple torque control of switched reluctance motor drives," *IEEE Trans. Power Electronics*, vol. 30, pp. 1457-1470, 2015.
[12] L. Yu, Z. Zhang, Z. Chen and Y. Yan, "Analysis and verification of the doubly salient brushless DC generator for automobile auxiliary power unit application," *IEEE Trans Ind. Electron.*, vol. 61, no. 12, pp. 6655-6663, Dec. 2014.
[13] Y. Wang, S. Niu and W. Fu, "Electrical-Continuously Variable Transmission System Based on Doubly Fed Flux-Bidirectional Modulation," *IEEE Trans Ind. Electron.*, vol. 64, no. 4, pp. 2722-2731, April 2017.
[14] X. Liu and Z. Q. Zhu, "Stator rotor pole combinations and winding configurations of variable flux reluctance machines," *IEEE Trans. Ind. Appl.*, vol. 50, no. 6, pp. 3675-3684, Nov.-Dec. 2014.
[15] S. Jia, R. Qu, J. Li, D. Li and H. Lu, "Design considerations of stator DC-winding excited vernier reluctance machines based on the magnetic gear effect," *IEEE Trans. Ind. Appl.*, vol. 53, no. 2, pp. 1028-1037, March-April 2017.
[16] M. Ehsani, I. Husain and A. B. Kulkarni, "Elimination of discrete position sensor and current sensor in switched reluctance motor drives," *IEEE Trans. Ind. Appl.*, vol. 28, no. 1, pp. 128-135, Jan.-Feb. 1992.
[17] J. Cai, Z. Liu, Y. Zeng, H. Jia and Z. Deng, "A Hybrid-Harmonic-Filter-Based Position Estimation Method for an SRM with Embedded Inductive Sensing Coils," *IEEE Trans. Power Electron.*, vol. 33, no. 12, pp. 10602-10610, Dec. 2018.
[18] J. Ye, B. Bilgin and A. Emadi, "Elimination of Mutual Flux Effect on Rotor Position Estimation of Switched Reluctance Motor Drives," *IEEE Trans. Power Electron.*, vol. 30, no. 3, pp. 1499-1512, March 2015.
[19] J. Cai and Z. Liu, "An Unsaturated Inductance Reconstruction Based Universal Sensorless Starting Control Scheme for SRM Drives," *IEEE Trans. Ind. Electron.*, vol. 67, no. 11, pp. 9083-9092, Nov. 2020.
[20] J. Cai and Z. Deng, "Sensorless Control of Switched Reluctance Motor Based on Phase Inductance Vectors," *IEEE Trans. Power Electron.*, vol. 27, no. 7, pp. 3410-3423, July 2012.
[21] G. Pasquesoone, R. Mikail and I. Husain, "Position Estimation at Starting and Lower Speed in Three-Phase Switched Reluctance Machines Using Pulse Injection and Two Thresholds," *IEEE Trans. Ind. Appl.*, vol. 47, no. 4, pp. 1724-1731, July-Aug. 2011.
[22] X. Zhou, B. Zhou, K. Wang, L. Zhang and Y. Zhao, "Two-Step Rotor Position Estimation Method for Doubly Salient Electromagnetic Starter-Generator Over Zero and Low Speeds Range," *IEEE J. Emerg. Sel. Topics Power Electron.*, vol. 9, no. 3, pp. 2664-2673, June 2021.
[23] Jianrong Bu and Longya Xu, "Eliminating starting hesitation for reliable sensorless control of switched reluctance motors," *IEEE Trans. Ind. Appl.*, vol. 37, no. 1, pp. 59-66, Jan.-Feb. 2001.
[24] M. Krishnamurthy, C. S. Edrington and B. Fahimi, "Prediction of rotor position at standstill and rotating shaft conditions in switched reluctance machines," *IEEE Trans. Power Electron.*, vol. 21, no. 1, pp. 225-233, Jan. 2006.
[25] L. Shen, J. Wu and S. Yang, "Initial Position Estimation in SRM Using Bootstrap Circuit Without Predefined Inductance Parameters," *IEEE Trans. Power Electron.*, vol. 26, no. 9, pp. 2449-2456, Sept. 2011.
[26] Y. Zhao, H. Wang, H. Zhang and L. Xiao, "Position-Sensorless Control of DC + AC Stator Fed Doubly Salient Electromagnetic Motor Covered Full Speed Range," *IEEE Trans. Ind. Electron.*, vol. 62, no. 12, pp. 7412-7423, Dec. 2015.
[27] X. Zhou and B. Zhou, "Rotor position estimating scheme for doubly salient EM machine sensorless startup," *IET Electron. Lett.*, vol. 53, no. 15, pp. 1033–1044, Jul. 2017.
[28] X. Zhou, B. Zhou and J. Wei, "A Novel Position-Sensorless Startup Method for DSEM *IEEE Trans. Ind. Appl.*, vol. 54, no. 6, pp. 6101-6109, Nov.-Dec. 2018.
[29] X. Zhou, B. Zhou and K. Wang, "Position Sensorless Control for Doubly Salient Electromagnetic Machine with Improved Startup Performance," *IEEE Trans. Ind. Electron.*, vol. 67, no. 3, pp. 1782-1791, March 2020.
[30] E. Ofori, T. Husain, Y. Sozer and I. Husain, "A Pulse-Injection-Based Sensorless Position Estimation Method for a Switched Reluctance Machine Over a Wide Speed Range," *IEEE Trans. Ind. Appl.*, vol. 51, no. 5, pp. 3867-3876, Sept.-Oct. 2015.

WEIYU WANG is currently working toward the Ph.D. degree in electrical engineering with the Department of Electrical Engineering, Hong Kong Polytechnic University, Hong Kong, China. His research interests include electrical machine drive and position-sensorless drive.

XING ZHAO (Member, IEEE) received the B.Eng. degree from Nanjing University of Aeronautics and Astronautics, Nanjing, China, in 2014, and the Ph.D. degree from The Hong Kong Polytechnic University, Hong Kong, China, in 2020, both in Electrical Engineering. From Jul. 2019 to Jan. 2020, he was a Visiting Research Scholar with the Center for Advanced Power Systems, Florida State University, Tallahassee, USA. Between Jul. 2020 and Oct. 2021, he served as a Research Assistant Professor with the Department of Electrical Engineering, The Hong Kong Polytechnic University. Since Nov. 2021, he has been a Lecturer in the Department of Electronic Engineering with University of York, UK. He has authored or coauthored more than 50 technical papers in the international journals and conferences and holds six granted patents. His research interests include advanced electrical machines, motor drives, and power electronics for electric vehicles and renewable energy systems. Currently he serves as an Associate Editor of IEEE Open Journal of Industrial Electronics Society.

SHUANGXIA NIU (Sennior Member, IEEE) received the B.Sc. and M.Sc. degrees in electrical engineering from the School of Electrical Engineering and Automation, Tianjin University, Tianjin, China, and the Ph.D. degree in electrical engineering from the Department of Electrical and Electronic Engineering, The University of Hong Kong, Hong Kong. Since 2009, she has been with The Hong Kong Polytechnic University, Hong Kong, where she is currently an Associate Professor with the Department of Electrical Engineering. She has authored or coauthored over 100 articles in leading journals. Her research interests include novel electrical machines and drives, renewable energy conversion systems, and applied electromagnetics.